

Computational Lithography and Computational Metrology for Nanomanufacturing

Shiyuan Liu

State Key Laboratory of Digital Manufacturing Equipment and Technology,
Wuhan National Laboratory for Optoelectronics, Huazhong University of Science and Technology,
Wuhan, China
E-mail: shyliu@mail.hust.edu.cn

Abstract – Nanomanufacturing refers to the manufacturing of products with feature dimensions at the nanometer scale. This paper presents the fundamental concepts and key issues of computational lithography and computational metrology for nanomanufacturing. We demonstrate their potentials and challenges by providing several examples carried out in our research group. We believe and expect that they will play a significant role in the future nanomanufacturing.

Keywords - nanomanufacturing; computational lithography; computational metrology; nanometrology; optical metrology; model-based metrology; optical proximity correction

I. INTRODUCTION

Nanomanufacturing refers to the manufacturing of products with feature dimensions at the nanometer scale. It is an essential bridge between the newest discoveries of fundamental nanoscience and real-world products by nanotechnology. For nanotechnology-enabled products to achieve broad impacts to society and to promise huge benefits to our everyday lives, they must be manufactured in market-appropriate quantities by reliable, repeatable, economical, and commercially viable methods [1].

It is well recognized that currently there are two paths for nanomanufacturing. One is the bottom-up method, or self-assembly method, and the other is the up-down method, which is based on nanoscale patterning [2]. Although the bottom-up method takes advantage of using the natural tendency of materials to spontaneously coalesce into shapes of technological importance without relying on any complex and expensive tools, the number of achievable shapes and workable materials is limited, which places severe restrictions on the types of nanostructures that can be achieved. As one of the most matured and sophisticated patterning methods, the optical lithography technique has been widely used for the high volume of conventional semiconductor manufacturing as well as novel nanomanufacturing. Nowadays, with the technology node reaching 45nm and 32nm, and even moving towards 22nm and below, the critical challenge for lithography-based nanomanufacturing is the requirements including predictive simulation of lithographic processes, optimal design of mask patterns, and in-line characterization of lens properties. Fortunately, the computational lithography technique provides a feasible and efficient approach to these requirements, by investigations of physical understanding, mathematical abstraction, and implementation simplification of real-world optical lithography [3].

Another most critical issue to the realization of nanomanufacturing is the development of necessary instrumentation and metrology at the nanoscale. The currently available metrology tools such as scanning probing microscope (SPM), transmission electron microscope (TEM), scanning electron microscope (SEM) and atomic force microscope (AFM), are capable of meeting the exploratory nanoscale research, but new nanotechnology industries that mass-produce products require high-performance, cost-effective, reliable instrumentation and improved measurement methods that meet the requirements of effective nanomanufacturing [4, 5]. The optics-based metrology tools, which have drawn more and more attention in semiconductor manufacturing because of their attractive advantages, such as low cost, non-contactness, non-destruction, and high throughput, may be one of the best choices. Overall, the optics-based metrology can be classified into two categories, namely the model-free and the model-based methods [6]. The model-free metrology, such as the conventional optical microscopy, directly determines the dimensional information from the “best-focus” images. However, due to the diffraction limit, it is difficult for the optical microscopy to obtain sharp images of the features smaller than half the wavelength of illumination (about 200 nm for the visible region) even at the best focus position. Therefore, this kind of WYSIWYG (what you see is what you get) metrology seems to be helpless for nanoscale dimensional analysis. In contrast, the model-based metrology, such as scatterometry, does not depend on the images with well defined edges and allows for the indirect determination of the geometrical parameters of the measuring targets from the measured signatures [7, 8]. Since this model-based metrology heavily relies on the forward optical modeling and the inverse parameter extraction, which are both computationally intensive, here we term this metrology as computational metrology. To the best of our knowledge, it is the first time we give this term similar to the case of computational lithography, with emphasis on solving the mathematical problems.

In this paper, I will present the fundamental concepts and key issues of computational lithography and computational metrology for nanomanufacturing. Their potentials and challenges are demonstrated by providing several examples carried out in our research group.

II. COMPUTATIONAL LITHOGRAPHY

The main physical components of a typical lithographic imaging system contains four elements, namely the

This project was funded by National Natural Science Foundation of China (Grant No. 91023032, 51005091, 50775090) and Fundamental Research Funds for the Central Universities of China (Grant No. 2010ZD004).

illumination source, the mask pattern, the pupil (projection lens), and the aerial image (or resist image), as shown in Fig.1 (a). Based on the Hopkins imaging theory [9], the image intensity at a space point \mathbf{x} can be written in terms of the pairs of spatial-frequencies of the object spectra $O(\mathbf{f}_1)$ and $O(\mathbf{f}_2)$, which respectively correspond to the Fourier transform (FT) of the mask function $m(\mathbf{x}_1)$ and $m(\mathbf{x}_2)$:

$$I(\mathbf{x}) = \iint O(\mathbf{f}_1)O^*(\mathbf{f}_2)TCC(\mathbf{f}_1, \mathbf{f}_2)\exp[-2\pi i(\mathbf{f}_1 - \mathbf{f}_2) \cdot \mathbf{x}]d\mathbf{f}_1d\mathbf{f}_2, \quad (1)$$

where \mathbf{f} , \mathbf{f}_1 , \mathbf{f}_2 are variables that are two-dimensional real vectors representing the normalized spatial-frequency pupil coordinates, and TCC is introduced as the concept of transmission cross-coefficient, which is expressed as:

$$TCC(\mathbf{f}_1, \mathbf{f}_2) = \int S(\mathbf{f})H(\mathbf{f} + \mathbf{f}_1)H^*(\mathbf{f} + \mathbf{f}_2)d\mathbf{f}, \quad (2)$$

where $S(\mathbf{f})$ is the effective source function, and $H(\mathbf{f})$ is the pupil function given by

$$H(\mathbf{f}) = P(\mathbf{f})\exp[-ikW(\mathbf{f})]. \quad (3)$$

Here, $P(\mathbf{f}) = \text{circ}(\mathbf{f})$ is the unaberrated pupil function, $k = 2\pi/\lambda$ is the wave number; λ is the wavelength of the monochromatic light source, and $W(\mathbf{f})$ is the aberrated wavefront.

According to the particular nanomanufacturing requirements including predictive simulation of lithographic processes, optimal design of mask patterns, and in-line characterization of lens properties, the aerial image intensity $I(\mathbf{x})$, the mask function $M(\mathbf{x})$ and the wavefront aberration $W(\mathbf{f})$ need to be both fast and accurately calculated. Therefore, as shown in Fig. 1 (b), the computational lithography involves three key issues and techniques, namely (1) the aerial image simulation, (2) the mask pattern optimization, and (3) the pupil phase retrieval. The aerial image simulation for a specific lithographic imaging system is a traditional forward process in computational lithography. The mask pattern optimization, which is well known as the inverse lithography technique, aims at deriving the optimal mask pattern for a desired image. The pupil phase retrieval can be treated as an extended inverse problem in computational lithography.

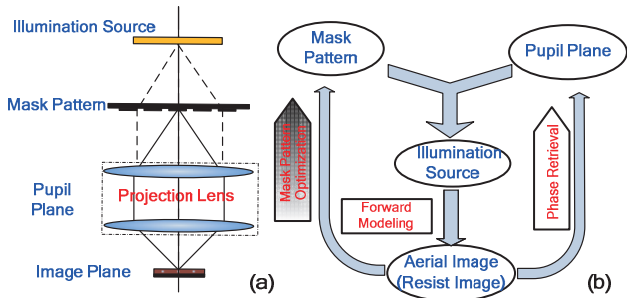


Figure 1. Principle of computational lithography.

A. Aerial Image Simulation

The aerial image simulation for a specific lithographic imaging system is a traditional forward process in computational lithography, with the combination of known variables of source, mask and pupil. The theories of aerial

image formation of the lithographic imaging system can be roughly categorized into the Abbe's theory and the Hopkins' theory. The Abbe's theory considers that the source is constructed by a number of incoherent source points. Thus, the total aerial image intensity can be treated as the superimposition of all the intensity caused by these source points. Although the Abbe's theory takes the advantage of representing the physical process of real imaging process directly, the computation speed of this method is limited because the fast Fourier transform (FFT) is needed for the intensity calculation of every source point. Therefore, it is time-consuming to obtain a high accuracy in aerial image simulation by the Abbe's theory. In contrast, in Hopkins' theory the partially coherent imaging formulation as shown in Eq. (1) has been widely used for the aerial image simulation. For the two-dimensional aerial image simulation, the Hopkins's formulation involves a quadruple integral over the pupil plane with a four-dimensional (4D) TCC.

The calculation of the 4D TCC matrix is a key step of the aerial image simulation. The fast TCC calculation algorithm can be mainly classified into the analytical algorithm and the matrix-based algorithm. The analytical algorithm is quite efficient and accurate as a key step for analytical aerial image formation. It was first proposed by Kintner for one-dimensional masks with circular aperture and aberration-free optics [10]. Subramanian extended this algorithm so that defocused image with square pupil could also be supported [11]. Most recently Yamazoe reported a matrix-based fast algorithm for TCC calculation according to Abbe's theory [12]. He introduced a matrix known as pupil shift matrix, and proved that the TCC matrix is simply the product of the pupil shift matrix and its Hermitian conjugate. Köhler provided another matrix-based TCC calculation algorithm based on the two-dimensional FFT since TCC can be treated as a generalized convolution in the frequency domain [13]. He also applied the poly-phase decomposition method to perform decimation which leads to a faster speed for bitmap apertures. Each of these algorithms has its advantages and disadvantages with a compromise necessary to achieve a balance between the accuracy and speed. As shown in Fig. 2, we present a slice of the 4D TCC calculation results conducted on the mainstream illumination sources commonly used in current lithographic tools.

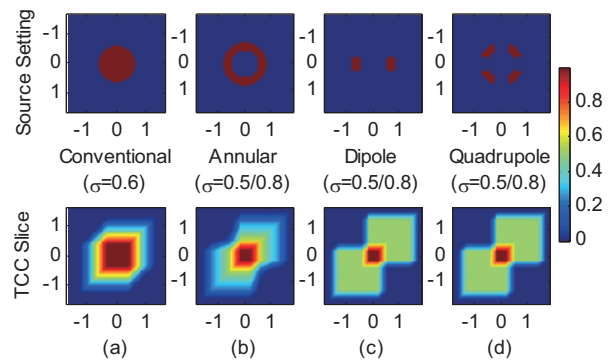


Figure 2. A slice of the 4D TCC calculation results conducted on the mainstream illumination configurations in current lithographic tools, including (a) conventional, (b) annular, (c) dipole, and (d) quadrupole sources.

Since the 4D TCC matrix contains all the information of the illumination source and the pupil where the aberrations and defocus of the optical system are included, the TCC matrix can be calculated only once for different mask patterns in the aerial image simulation. It is thus possible to decompose the 4D TCC matrix into a fewer kernels in advance, and then these kernels are used to speed up the aerial image calculation. This method for partially coherent imaging systems is referred to as the optimal coherent approximations (OCA) or more commonly as the sum of coherent system decomposition (SOCS) [14, 15], in which the TCC matrix is decomposed into eigenvalues and eigenfunctions by singular-value decomposition (SVD):

$$TCC(\mathbf{f}_1, \mathbf{f}_2) = \sum_{n=1}^{\infty} \lambda_n \varphi_n(\mathbf{f}_1) \varphi_n^*(\mathbf{f}_2), \quad (4)$$

where n indicates the n th order decomposition, λ_n is the eigenvalue, and $\varphi_n(\mathbf{f})$ is the eigenfunction. Figure 2 depicts the first 6 eigenfunctions in a lithographic imaging system with a circular source ($\sigma=0.5$) and aberration-free pupil.

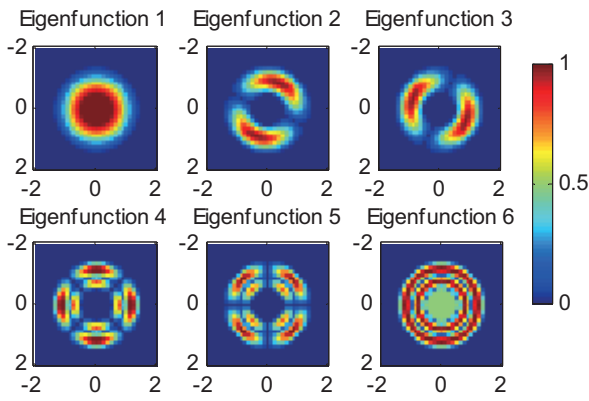


Figure 3. The first 6 eigenfunctions of an optical imaging system with a circular source ($\sigma=0.5$) and free-aberration pupil.

It is noted that the eigenvalues decrease rapidly with the order increasing, it is thus possible to only use the first few N eigenvalues and eigenfunctions (called optical kernels) to approximate the aerial image calculation with high accuracy:

$$I(\mathbf{x}) = \sum_{n=1}^N \lambda_n |\text{FT}[\varphi_n(\mathbf{f})O(\mathbf{f})]|^2, \quad (5)$$

where FT denotes the Fourier transform.

B. Mask Pattern Optimization

The mask pattern optimization aims at deriving the optimal mask pattern for a desired image with the combination of known variables of source and pupil. The desired image is usually the given resist image, which can be treated as a natural extension of the aerial image by considering the resist effect. Therefore, the imaging formation process can be mathematically expressed as [16]:

$$z(\mathbf{x}) = T\{m(\mathbf{x})\}, \quad (6)$$

where $T\{\cdot\}$ is the forward model such as Eq. (5) which maps the input mask function $m(\mathbf{x})$ into the output resist image function $z(\mathbf{x})$. Thus, the mask pattern optimization can be

treated as the well-known inverse lithography technique which is beneficial in creating a both physically realizable and functionally adequate mask pattern:

$$\hat{m}(\mathbf{x}) = \arg \min_{m(\mathbf{x})} d[z^*(\mathbf{x}), T\{m(\mathbf{x})\}]. \quad (7)$$

Here, $z^*(\mathbf{x})$ is the desired output resist image. The problem is to seek a pre-distorted input mask function $m(\mathbf{x})$ with an output $z(\mathbf{x})=T\{m(\mathbf{x})\}$ that is mostly close to the desired output $z^*(\mathbf{x})$. This can be achieved by searching the space of inputs and choosing the $m(\mathbf{x})$ which minimizes the distance $d[z^*(\mathbf{x}), z(\mathbf{x})]$. Since the mask pattern to be determined is represented by a gray-level image and unconstrained by the topology of the original physical design, the inverse lithography technique generally promises to deliver superior pattern fidelity over the existing model-based optical proximity correction (OPC) approaches. As shown in Fig. 4, we present a simulation result of pixel-based mask optimization using the steepest gradient algorithm. It is clear that both of the optimized gray mask and binary mask demonstrate a great improvement in fidelity with the desired pattern.

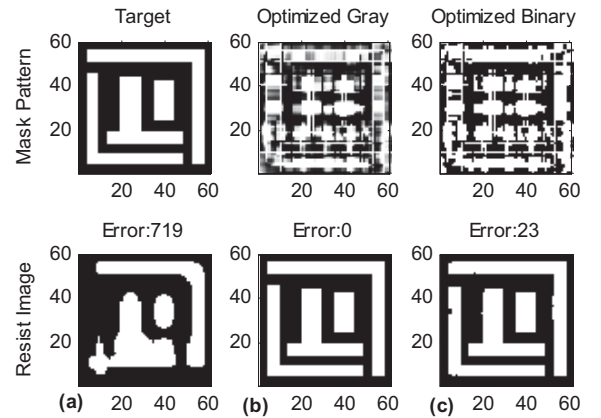


Figure 4. Results of mask optimization through inverse lithography technique, (a) is the result of initial mask which equal to the target pattern, (b) and (c) are the optimized gray mask and binary mask, respectively.

One of the most critical issues in mask pattern optimization is to achieve both of the mathematical description for physical modeling and the mask regularization that provides suitable control of lithography robustness and mask manufacturability [3]. As shown in Fig. 4, the pixel-based algorithm in inverse lithography technique leads to the flexible mask transform and thus increases the complexity of optimized mask patterns and fabrication difficulty. Therefore, regularization terms are highly desired to guarantee the optimized mask pattern to be binary and less complex:

$$\hat{m}(\mathbf{x}) = \arg \min_{m(\mathbf{x})} (d(z^*(\mathbf{x}), T\{m(\mathbf{x})\}), R\{m(\mathbf{x})\}), \quad (8)$$

where $R\{m(\mathbf{x})\}$ is the regularization term. Generally, the regularization terms include quadratic penalty which guarantee the optimized mask pattern to be binary, and complexity terms such as total variation penalty and wavelet penalty which constrain the topology of the optimized mask [16-18]. As shown in Fig. 5, we present some examples of mask optimization with these regularization terms. By introducing

the quadratic penalty regularization term as shown in Fig. 5(a), the simulation result achieves an excellent fidelity of binary mask, but also generates intricate pattern topology. The total variation penalty regularization term is subsequently added to suppress the isolated holes, protrusions and jagged edges, and as shown in Fig. 5(b), this kind of penalty is noted to force the pattern changes to be spatially smoother and less abrupt. The effect of wavelet penalty regularization term is shown in Fig. 5(c), which provides another significant approach to remove the unwanted details such as small peaks and makes the shape of the blocks constructing the mask more regular. Although tiny pattern error appears when introducing the complexity penalty terms, the manufacturability of the mask pattern is improved greatly.

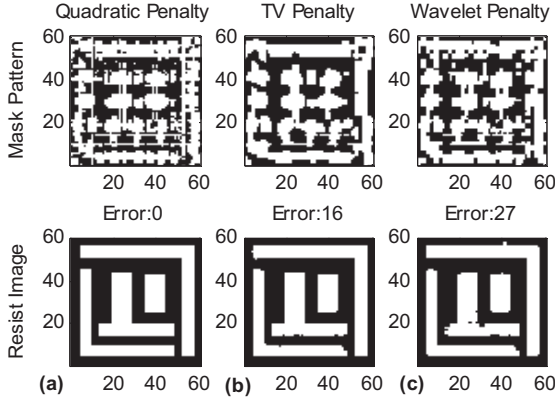


Figure 5. Results of mask pattern optimization using regularization terms.

C. Pupil Phase Retrieval

The pupil phase retrieval is an equivalent concept of characterizing the amount of lens aberration in lithographic imaging systems, with the combination of known parameters of source, mask, and aerial image. The Zernike series representation is useful as it provides explicit expressions for the well-known low order aberrations such as spherical, coma, astigmatism, etc., while higher-order polynomials are less significant in the description of aberrations [19, 20]. However, in order to meet the requirement of optical path tolerances on the order of several nanometers over extremely large aperture of current projection lens, the higher-order coefficients of Zernike polynomials are becoming increasingly important for monitoring lens performance on a regular basis. Moreover, in the current optical lithography processes for semiconductor manufacturing, partial coherent illumination sources have been widely used for the need of stringent critical dimension (CD) control. Therefore, it is highly desirable to develop a novel technique for in situ measurement of lens aberrations up to the 37th (or even higher-order) Zernike coefficient in lithographic tools with partially coherent illumination sources and arbitrarily shaped illumination sources.

Similar to the mask pattern optimization, the pupil phase retrieval can be treated as an extended inverse problem in computational lithography technique:

$$\hat{W}(\mathbf{f}) = \arg \min_{W(\mathbf{f})} d(I^*(\mathbf{x}, D), T\{W(\mathbf{f}); O(\mathbf{f}), D\}). \quad (9)$$

where D is the defocus value (in nanometer) of the image plane, $T\{\cdot\}$ is the forward model such as Eq. (5) which maps the input wavefront aberration $W(\mathbf{f})$ into the output aerial image (or resist image) $I(\mathbf{x}, D)=T\{W(\mathbf{f}); O(\mathbf{f}), D\}$ for a special mask pattern spectrum $O(\mathbf{f})$ at a certain defocus value D , and $I^*(\mathbf{x}, D)$ is the measured aerial image (or resist image). Compared to the ill-posed inverse problem in the mask pattern optimization, the solution of the inverse problem in pupil phase (or lens aberration) retrieval has the properties of existence and uniqueness based on a set of aerial images (or resist images) corresponding to multiple defocus values. In addition, by using specially designed mask patterns such as a set of binary gratings with different pitches and orientations, the nonlinear model $T\{\cdot\}$ can be physically and mathematically simplified as a linear relationship between the wavefront aberration and the first-order spectrum of the aerial image [21].

Recently, we proposed an aerial image based aberration measurement technique with generalized formulations suitable for arbitrarily shaped illumination sources by further derivation of the analytical aberration sensitivities based on the Hopkins theory of partially coherent imaging [22]. The aberration sensitivities can be categorized into odd and even types, each of which is presented as an aberration sensitivity function determined by independent variables of the Zernike order, source distribution and pupil position. With a set of Zernike orders, these aberration sensitivities can be considered as a set of analytical kernels which succeed in forming a sensitivity function space for aberration measurement under arbitrarily shaped illumination sources. As shown in Fig. 6, by the expansion of measurable information of through-focus images into the sensitivity function space, Zernike coefficients up to the 37th order can be conveniently obtained by the least-square method. Figure 7 illustrates the aberration measurement (pupil phase retrieval) results for the quadrupole illumination source. This aerial image based aberration measurement technique has been proved to be simple in implementation and yield a superior quality of in-line monitoring of imaging performance of current lithographic tools for nanomanufacturing.

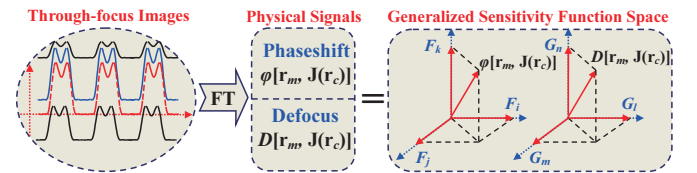


Figure 6. Expansion of the measurable information of through-focus images in the generalized sensitivity function space.

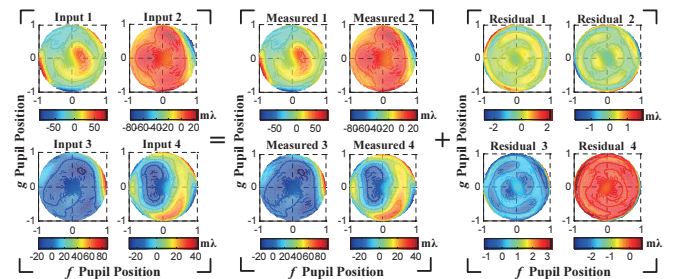


Figure 7. Results of pupil phase retrieval by aerial image based technique.

III. COMPUTATIONAL METROLOGY

In this section, we take the scatterometry as a particular example to demonstrate the fundamental concept and key issues of computational metrology for nanomanufacturing. The scatterometry is based on the conventional reflectometry or spectroscopic ellipsometry (SE), in which a collimated beam that is polarized in a known state and projected onto the sample, and the state of polarization of the reflected wave is analyzed. From the incident and reflected states of polarization, the intensity of the reflected light under different states of polarization, or the ratio of complex coefficients for the incident orthogonal linear polarizations parallel and perpendicular to the plane of incidence are determined [7, 8]. These output parameters are subsequently related to the structural and optical properties of the ambient-sample interface region by invoking an appropriate model and the electromagnetic theory of reflection. Eventually, the model parameters of interest can be determined by solving the corresponding inverse problem. The principle of computational metrology is illustrated in Fig. 8, with two key techniques involved, namely the forward modeling and the inverse problem solving.

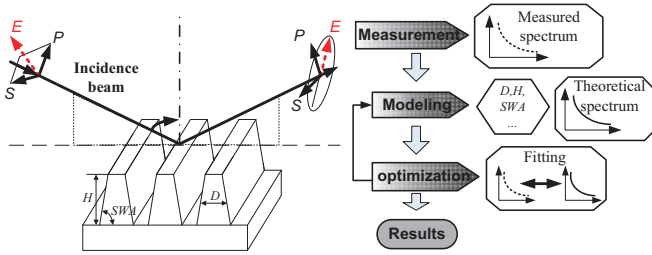


Figure 8. Principle of computational metrology.

Because the computational metrology is not operated in an imaging mode, an appropriate model based on classical electromagnetic theory which properly accounts for the physical essence of the scattering process is indispensable to determine the feature of the measured target. In particular, when the computational metrology is used to characterize the optical and structural properties of the interfacial region, a stratified-medium model (SMM) such as the two-phase model and the three-phase model that contains the appropriate parameters of the sample is required. More complexity can be built into the basic SMMs to represent such finer details as the interfacial roughness and phase mixing, a damage surface layer caused by polishing, or the possible presence of an outermost contamination film [23]. As for samples with periodic properties, the rigorous coupled wave analysis (RCWA) is always the best choice for the optical modeling [24, 25]. The effective medium theory (EMT) is used to calculate the dielectric functions of mixed phase based on their microstructure and components fractions, and sometimes EMT may be employed to simplify the modeling [26, 27]. Based on the established models, different optical responses can be obtained by choosing an appropriate measurement configuration such as the angle of incidence θ , the incident wavelength λ , and the azimuthal angle ϕ of the sample. Without losing generality, the optical response or the output parameters in computational metrology can be characterized by

the forward model $T\{\cdot\}$ with a formulation as:

$$\mathbf{y}(\lambda, \theta, \phi) = T\{\mathbf{s}; \lambda, \theta, \phi\}. \quad (10)$$

Here, \mathbf{s} denotes the structural and optical parameters of the sample such as CD, height, side wall angle (SWA), pitch, and refractive index; \mathbf{y} is the output parameters of the model. For the reflectometry, \mathbf{y} denotes the scalar of reflectance:

$$R = \frac{r_p r_p^* + r_s r_s^*}{2}, \quad (11)$$

and in the case of SE, \mathbf{y} denotes the ratio ρ of the complex reflection coefficients for the p and s polarizations r_p, r_s :

$$\rho = \tan \psi \exp(i\Delta) = \frac{r_p}{r_s}. \quad (12)$$

Apart from the forward modeling requirement, some inverse problem solving techniques, typically the library search method and the nonlinear regression method are employed for the reconstruction of the structural parameters of the sample in the computational metrology. In the library search method, the library is produced in advance by evaluating the forward model on a grid which covers the expected range of variation in the parameters [28]. At run time, the measured signature is compared to each signature in the library and the measurement output is the set of parameters used to generate the signature with the best fit to the measurement. However, the library method needs huge resource cost in computation and storage space, as the evaluation grid needs to be dense enough to produce measurement output with enough resolution. The nonlinear regression methods such as local optimization algorithms are widely used for grating metrology and design [29, 30]. The iteration process with the local optimization algorithm can be finished in several iterations, but it heavily depends on the initialization. It is well understood that the optimization is non-convex, and the iterative methods can easily lead to a local rather than global solution. Therefore, different optimization algorithms can be combined to promote their advantages.

In each of the inverse problem solving techniques, the values of the model parameters are sought so that the outputs of the model are best matched the measured ones. We describe this inverse problem in computational metrology with a formulation similar to that in the computational lithography:

$$\hat{\mathbf{s}} = \arg \min_{\mathbf{s} \in \mathbf{K}} d[\mathbf{y}^*(\lambda, \theta, \phi), T\{\mathbf{s}; \lambda, \theta, \phi\}], \quad (13)$$

where d denotes the distance between the measured output $\mathbf{y}^*(\theta, \lambda, \phi)$ and the modeled output $\mathbf{y}(\theta, \lambda, \phi) = T\{\mathbf{s}; \theta, \lambda, \phi\}$. Therefore, the computational metrology mainly involves the integration of the following three tasks: (1) measurement of the optical response under a certain optical configuration, (2) calculation of the theoretical optical response using an appropriate electromagnetic model; and (3) solving the inverse problem to determine model parameters that best match the measured and calculated optical responses.

Here we take the model-based infrared reflectometry (MBIR) as an instance to illustrate the above two key techniques [31, 32]. The MBIR, which can be considered to be

a particular form of scatterometry, is an attractive optical metrology that has been introduced recently for measuring high aspect-ratio periodic trench structures. We have successfully applied the MBIR technique in measuring a bottle trench structure, which is etched on the silicon substrate and filled with polysilicon as electrodes. This bottle trench structure is a typical design in advanced dynamic random access memory (DRAM) capacitors characterized by four geometric parameters: width of neck layer d_1 , depth of neck layer h_1 , width of bottle layer d_2 , and depth of bottle layer h_2 , as shown in Fig. 9. We modeled the structure as a two-layer stack and calculated the effective refractive index of each effective layer with a corrected effective medium approximation (EMA) method [31].

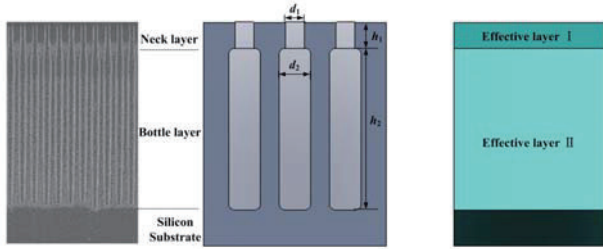


Figure 9. SEM micrograph of the bottle trench structure and its effective optical model.

An experimental platform has been set up to measure the reflectance spectral signals. The smooth part of the measured spectrum is utilized and the artificial neural network (ANN) and Levenberg-Marquardt (LM) algorithm are combined to extract parameters of the bottle trench structure, as shown in Fig. 10. Firstly, an ANN of multilayer perceptron (MLP) type is constructed. Then the ANN is trained by the back-propagation learning algorithm, which is classified as a supervised learning algorithm. Finally, the raw data of the measured reflectance spectrum R_m is processed by the trained ANN, which provides an output of the geometric parameter vector P with a few percentage of error. This output of ANN is then set as the initial estimate of the LM algorithm, which performs only a few iterations and further refines to an accurate final solution. Figure 11 depicts the fitted reflectance spectrum calculated from the extracted parameters compared to the measured reflectance spectrum [32].

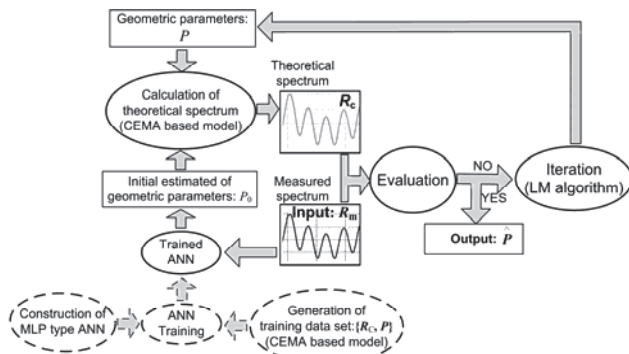


Figure 10. Flowchart of parameter extraction using the ANN and LM combined method.

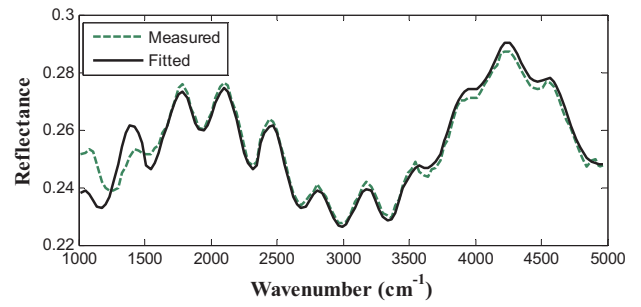


Figure 11. Measurement result of a bottle trench structure by the model-based infrared reflectometry.

Although the conventional SE has been widely used in the real-time characterization of depths of thin films as well as in the in-situ measurement of CD, SWA and overlay of nanostructures, it can only obtain two parameters, i.e., the amplitude ratio $\tan\psi$ and the phase shift difference Δ , during each measurement. In contrast, the Mueller matrix polarimetry (MMP) can obtain up to 16 parameters of the 4×4 Mueller matrix during each measurement [8, 33]. Consequently, the MMP can obtain much more useful information about the sample than the conventional SE, and thus has potential capability for the future line edge roughness (LER) and line width roughness (LWR) metrology in nanomanufacturing. As shown in Fig. 12, we present an example of sensitivity analysis of the MMP for nanostructure metrology.

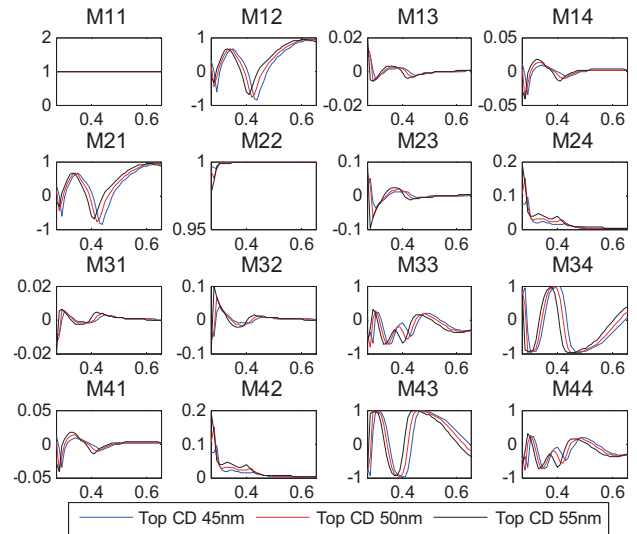


Figure 12. Calculated optical responses of Mueller matrix polarimetry for a two-dimensional nanostructure with square holes in 300nm thick photoresist. The periods in both directions are 100nm and the top CD of the holes is set to be 45nm, 50nm, and 55nm, respectively.

IV. CONCLUSIONS

In summary, both of the computational lithography and computational metrology involve two key techniques, namely the forward optical modeling and the inverse problem solving. As these two techniques both require intensive calculations, the success of computational lithography and computational metrology relies heavily on the accurate and fast forward

modeling methods as well as the robust and fast inverse optimization algorithms, both of which still remain as a challenge. By providing several initial examples carried out in our research group, we believe and expect that both of the computational lithography and computational metrology will play a significant role in the future nanomanufacturing.

ACKNOWLEDGMENT

The author would like to acknowledge all of his graduate students for their hard work at Nanoscale and Optical Metrology Group in Huazhong University of Science and Technology. Particular acknowledgments go to Dr. Chuanwei Zhang, Mr. Wei Liu, Mr. Xiuguo Chen, and Mr. Xiaofei Wu for their assistance in preparing the simulation results for this paper.

REFERENCES

- [1] G. Chryssolouris, P. Stavropoulos, G. Tsoukantas, K. Salonitis, and A. Stourmaras, "Nanomanufacturing process: a critical review," *Int. J. Mater. Prod. Technol.*, vol. 21, pp. 331-348, 2004.
- [2] H. Sengul, T. L. Theis, and S. Ghosh, "Toward sustainable nanoproducts: an overview of nanomanufacturing methods," *J. Ind. Ecol.*, vol. 12, pp. 329-359, 2008.
- [3] E. Y. Lam and A. K. Wong, "Computation lithography: virtual reality and virtual virtuality," *Opt. Express*, vol. 17, pp. 12259-12268, 2009.
- [4] K. W. Lyons and M. T. Postek, "Metrology at the nanoscale: what are the grand challenges?" in *Proc. SPIE*, 2008, vol. 7042, 704202.
- [5] M. T. Postek and K. Lyons, "Instrumentation, metrology, and standards: key elements for the future of nanomanufacturing," in *Proc. SPIE*, 2007, vol. 6648, 664802.
- [6] P. Weidner, A. Kasic, T. Hingst, C. Ehlers, S. Philipp, T. Marschner, and M. Moert, "Model-free and model-based methods for dimensional metrology during the lifetime of a product," in *Proc. SPIE*, 2008, vol. 7155, pp. 1550-1550.
- [7] H. T. Huang and F. L. Terry, "Spectroscopic ellipsometry and reflectometry from gratings (scatterometry) for critical dimension measurement and in situ, real-time process monitoring," *Thin Solid Films*, vol. 468, pp. 338-346, 2004.
- [8] M. Losurdo, M. Bergmair, G. Bruno, D. Cattelan, C. Cobet, A. D. Martino, et al., "Spectroscopic ellipsometry and polarimetry for materials and systems analysis at the nanometer scale: state-of-the-art, potential, and perspectives," *J. Nanopart. Res.*, vol. 11, pp. 1521-1554, 2009.
- [9] H. Hopkins, "On the diffraction theory of optical images," *Proc. R. Soc. A*, vol. 217, pp. 408-432, 1953.
- [10] E. Kintner, "Method for the calculation of partially coherent imagery," *Appl. Opt.*, vol. 17, pp. 2747-2753, 1978.
- [11] S. Subramanian, "Rapid Calculation of defocused partially coherent images," *Appl. Opt.*, vol. 20, pp. 1854-1857, 1981.
- [12] K. Yamazoe, "Computation theory of partially coherent imaging by stacked pupil shift matrix," *J. Opt. Soc. Am. A*, vol. 25, pp. 3111-3119, 2008.
- [13] R. Köhle, "Fast TCC algorithm for the model building of high NA lithography simulation," in *Proc. SPIE*, 2004, vol. 5754, pp. 918-929.
- [14] Y. C. Pati and T. Kailath, "Phase-shifting masks for microlithography: automated design and mask requirements," *J. Opt. Soc. Am. A*, vol. 11, pp. 2438-2452, 1994.
- [15] N. B. Cobb, "Fast optical and process proximity correction algorithms for integrated circuit manufacturing," Ph.D. dissertation, Univ. of California Berkeley, 1998.
- [16] A. Poonawala and P. Milanfar, "Mask design for optical microlithography - an inverse imaging problem," *IEEE Trans. Image Process.*, vol. 16, pp. 774-788, 2007.
- [17] X. Ma and G. R. Arce, "Generalized inverse lithography methods for phase-shifting mask design," *Opt. Express*, vol. 15, pp. 15066-15079, 2007.
- [18] X. Ma and G. R. Arce, "PSM design for inverse lithography with partially coherent illumination," *Opt. Express*, vol. 16, pp. 20126-20141, 2008.
- [19] F. Zernike, "Beugungstheorie des Schneidverfahrens und seiner verbesserten form, der Phasenkontrastmethode," *Physica*, vol. 1, pp. 689-704, 1934.
- [20] M. Born and E. Wolf, *Principles of Optics*, 7th ed. Pergamon, 1999, chap. 9.
- [21] W. Liu, S. Y. Liu, T. T. Zhou, and L. J. Wang, "Aerial image based technique for measurement of lens aberrations up to 37th Zernike coefficient in lithographic tools under partial coherent illumination," *Opt. Express*, vol. 17, 19278-19291, 2009.
- [22] W. Liu, S. Y. Liu, T. L. Shi, and Z. R. Tang, "Generalized formulations for aerial image based lens aberration metrology in lithographic tools with arbitrarily shaped illumination sources," *Opt. Express*, vol. 18, pp. 20096-20104, 2010.
- [23] R. M. A. Azzam, "Ellipsometry," in *Handbook of Optics*, 3rd ed, vol. 1. M. Bass and V. N. Mahajan, Eds, McGraw Hill, 2010, pp. 16.1-16.25.
- [24] M. G. Moharam and T. K. Gaylord, "Rigorous coupled-wave analysis of planar-grating diffraction," *J. Opt. Soc. Am.*, vol. 71, pp. 811-818, 1981.
- [25] M. G. Moharam, E. B. Grann, and D. A. Pommet, "Formulation for stable and efficient implementation of the rigorous coupled-wave analysis of binary gratings," *J. Opt. Soc. Am. A*, vol. 12, pp. 1068-1076, 1995.
- [26] T. C. Choi, *Effective Medium Theory: Principles and Applications*. Oxford University Press, 1999.
- [27] S. M. Rytov, "Electromagnetic properties of a finely stratified medium," *Sov. Phys. JETP*, vol. 2, pp. 466-475, 1956.
- [28] X. Niu, N. Jakatdar, J. Bao, and C. J. Spanos, "Specular spectroscopic scatterometry," *IEEE Trans. Semicond. Manuf.*, vol. 14, pp. 97-111, 2001.
- [29] R. T. Zheng, N. Q. Ngo, L. N. Binh, and S. C. Tjin, "Two-stage hybrid optimization of fiber Bragg gratings for design of linear phase filters," *J. Opt. Soc. Am. A*, vol. 21, pp. 2399-2405, 2004.
- [30] K. Hehl, J. Bischoff, U. Mohaupt, et. al., "High-efficiency dielectric reflection gratings: design, fabrication, and analysis," *Appl. Opt.*, vol. 38, pp. 6257-6271, 1999.
- [31] C. W. Zhang, S. Y. Liu, T. L. Shi, and Z. R. Tang, "Fitting-determined formulation of effective medium approximation for 3D trench structures in model-based infrared reflectometry," *J. Opt. Soc. Am. A*, vol. 28, pp. 263-271, 2011.
- [32] C. W. Zhang, S. Y. Liu, T. L. Shi, and Z. R. Tang, "Improved model-based infrared reflectometry for measuring deep trench structures," *J. Opt. Soc. Am. A*, vol. 26, pp. 2327-2335, 2009.
- [33] T. Novikova, A. D. Martino, P. Bulkin, Q. Nguyen, and B. Drévilion, "Metrology of replicated diffractive optics with Mueller polarimetry in conical diffraction," *Opt. Express*, vol. 15, pp. 2033-2046, 2007.